This is an open access article published under an ACS AuthorChoice License, which permits copying and redistribution of the article or any adaptations for non-commercial purposes.

ACS OMEGA

Article

Cite This: ACS Omega 2019, 4, 14057−14066

http://pubs.acs.org/journal/acsodf

Simultaneous Recovery of Display Panel Waste Glass and Wastewater Boron by Chemical Oxo-precipitation with Fluidized-Bed Heterogeneous Crystallization

Cheng-Kuo Tsai,[†,‡] Nien-Tsu Lee,[‡] Gaw-Hau Huang,[‡] Yoshikazu Suzuki,[§] and Ruey-an Doong*[,†]

[†]Department of Biomedical Engineering and Environmental Sciences, National Tsing Hua University, 101, Sec. 2, Kuang Fu Road, Hsinchu 30013, Taiwan

[‡]Department of Chemical Analysis, Industrial Technology Research Institute (ITRI), Hsinchu 30011, Taiwan

[§]Faculty of Pure and Applied Sciences, University of Tsukuba, Ibaraki 305-8573, Japan

Supporting Information

ABSTRACT: Silica-based carrier is a promising material for recovery of metal and nonmetal contaminants in chemical oxo-precipitation-fluidized bed crystallization (COP-FBC) system. Boron species are an essential element for plant growth and can cause health concerns in human beings at high concentrations in water environments. The composition of thin-film transistor liquid crystal display (TFT-LCD) contains a wide variety of metal oxides and can be tailored as promising functional mesoporous carriers for boron crystallization recovery in the presence of barium ions and hydrogen peroxide. In this study, waste-derived mesoporous aluminosilicate (MAS) nanomaterial in the presence of barium ions and hydrogen peroxide was used as a carrier for sustainable recovery of crystallized boron, a priority wastewaters pollutant. The MAS shows the hierarchically homogeneous distribution of nanostructured aluminosilicate particles with an average size of 12.8 ± 3.6 nm on the surface after the activation with Na_2CO_3 at 1000 °C. Moreover, the negatively charged surface and the mesoporous structure of MAS enhance the adsorption of Ba^{2+} onto MAS, and the Langmuir adsorption capacity of 105 mg/g is achieved, which is conducive to the enhancement of the recovery of boron species. Moreover, the recovery efficiency and crystallization ratio of boron by MAS can be up to 84.5 and 93.4%, respectively. The cross-sectional scanning electron microscopy images and the high-temperature X-ray diffraction results confirm the boron recovery mechanism that the negatively charged functional group as well as the mesoporosity of MAS triggers the rapid formation of needle-shaped precipitates of barium peroxoborate, and then converted to barium borate after calcination at 1050 °C. Results obtained in this study clearly demonstrate the possibility of fabricating environmentally benign mesoporous aluminosilicate adsorbents from TFT-LCD waste to sustainably recover and crystallize boron species from water and wastewater in COP-FBC.

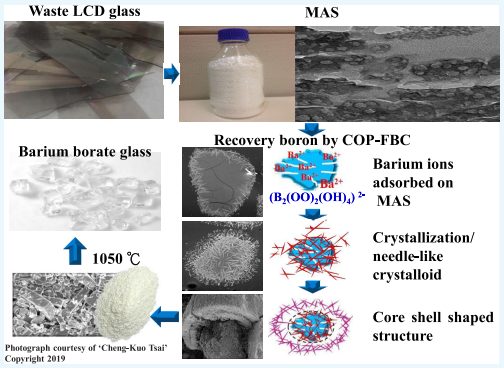

INTRODUCTION

Boron (B) is an element with a number of complex compounds such as boric acid, borate, and perborate in hydrosphere and lithosphere.[1] These compounds are commonly used in a wide variety of industrial purposes and result in increased environmental concerns after their release into water bodies.[2,3] Usually, highly soluble boron elements are easily associated with charged molecules, making boron species extremely difficult to be harvested from water and wastewater.[3] Although boron is an essential element for plant growth, the long-term exposure to high concentrations of boron would result in toxic effects on human health such as coronary artery, cardiovascular, and nervous systems.[2,4,5] Due to its possible hazard on human beings and ecology, boron has been promulgated as a priority pollutant and the guideline level in drinking water is 2.4 mg/L by the World Health Organization.[4,5] Consequently, the need of control technology for an effective recovery of boron as well as conversion of precipitates into high-value products gives rise to the development of sustainable technology for boron treatment and recovery.

Over the past decades, several technologies have been employed for the removal of boron species from effluent streams, namely, chemical precipitation,[6,7] electrocoagulation,[8,9] ion exchange,[10] adsorption,[11,12] chemical oxo-precipitation (COP),[13,14] and COP with fluidized-bed homogeneous crystallization (COP-FBHC).[15] COP is the peroxolysis process of boron species, which combines oxidant and chemical precipitation for precipitate transformation from $BaB(OH)_3OOB(OH)_3$ and $Ba(B(OH)_3OOH)_2$ to the crystallized $BaB(OH)_2(OO)_2B(OH)_2$ at room temperature,[14−16] COP is an efficient method for the treatment of elevated concen-

Received: June 25, 2019
Accepted: August 2, 2019
Published: August 16, 2019

Downloaded via UNIV OF TSUKUBA on June 18, 2020 at 01:40:56 (UTC).
See https://pubs.acs.org/sharingguidelines for options on how to legitimately share published articles.

Scheme 1. Illustration of the Crystallization Mechanism for the Recovery of Boron Species Using Mesoporous Aluminosilicate (MAS) as a Carrier in a Chemical Oxo-precipitation Fluidized Bed Crystallization (COP-FBC) Reactor[a]

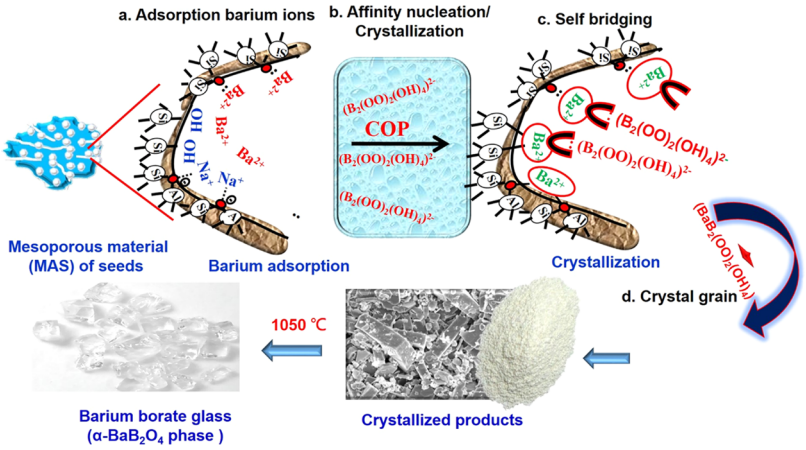

[a]Photograph courtesy of "Cheng-Kuo Tsai". Copyright 2019.

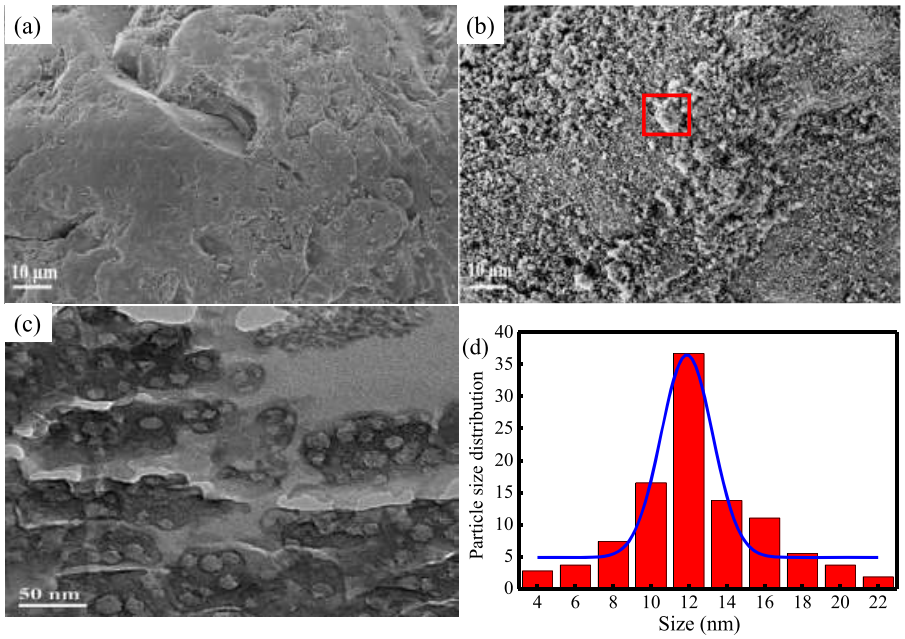

Figure 1. SEM images of (a) silica sand and (b) MAS nanomaterial, (c) cross-sectional FE-TEM image of MAS, and (d) particle size distribution of MAS.

trations of boron in comparison with the chemical precipitation. Usually, the addition of divalent metal salts such as calcium (Ca^{2+}), magnesium (Mg^{2+}), and barium (Ba^{2+}) along with H_2O_2 is needed to promote the formation of metal perborate. Barium ions are regarded as the most suitable ions because of the formation of barium perborate.[17] Although COP and COP-FBHC exhibit good efficiency in the recovery of high concentrations of boron, several challenges including the production of high water content sludge[13] and the difficulty in the disposal of sludge are experienced because of the homogeneous precipitation process.

To overcome the disadvantage of producing large amounts of sludge, COP with fluidized-bed crystallized (COP-FBC), a heterogeneous crystallization using active silica-based particles as carriers in COP reactor, has been developed to reduce the produced amount of sludge as well as to enhance the crystallization ratio.[18,19] Several studies have shown that FBC has a good removal and crystallization efficiency on the removal of nonmetal elements such as phosphorous[18] and fluoride.[19] However, the sand carriers used in COP-FBC are usually nonporous and have a low surface area, which is relatively difficult in promoting the nucleation for boron recovery in the presence of Ba^{2+}. It is noted that several mesoporous materials including SBA-15,[20] MCM-41,[21] and titanate nanotubes[22,23] have been used to adsorb divalent metal ions. However, the use of mesoporous materials as carriers for COP-FBC to effectively remove boron as well homogeneously crystallize boron-based precipitates in the presence of divalent metal ions has received less attention. It is therefore imperative to look for cost-effective mesoporous materials as COP-FBC carrier to rapidly recover boron by crystallization of boron species in the presence of barium ions.

TFT-LCD panel contains a high content of valuable material including glass, plastic and precious metals and different

DOI: 10.1021/acsomega.9b01900
ACS Omega 2019, 4, 14057−14066

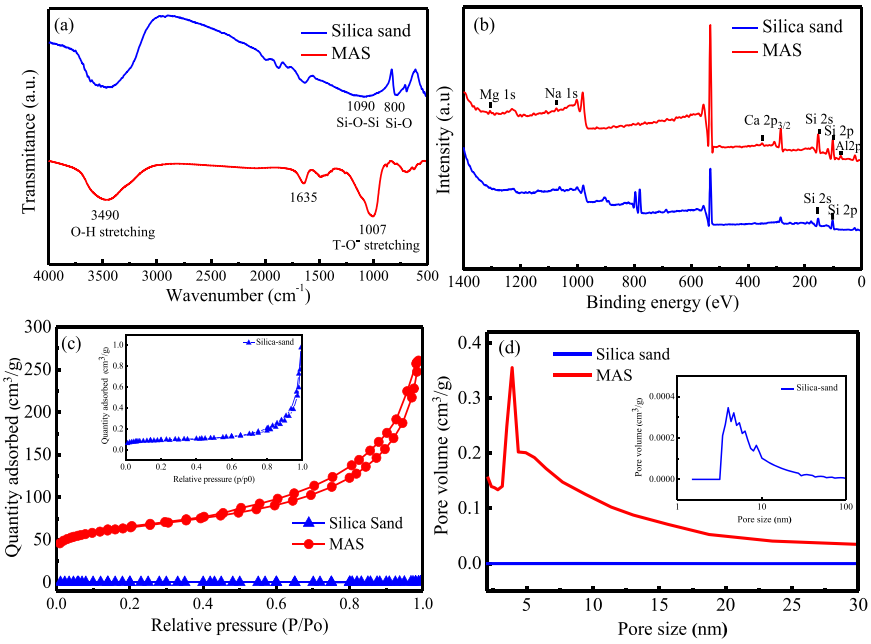

Figure 2. (a) FTIR spectra of silica and MAS, (b) X-ray photoelectron spectra (XPS) of silica and MAS, and (c) N_2 adsorption−desorption isotherm and (d) pore size distribution of the commercial silica sand and the as-prepared MAS nanomaterials derived from the waste TFT-LCD. Insets in figure (c) and (d) are the enlarged figures of isotherm and pore size distribution of silica sand, respectively.

approaches for the recovery of glass from end-of-life liquid crystal display[24,25] such as zeolite[26] and soda lime silicate glasses.[27] Usually, TFT-LCD can undergo thermoalkaline treatment and the impurities like metal and metal oxides can be removed by acid washing.[28] However, the fabrication of silica-based mesoporous materials from TFT-LCD has received less attention. A previous study has indicated that a mesoporous aluminosilicate composite can be prepared from the TFT-LCD waste panel for an effective adsorption of heavy metal ions including Ni, Cu, and Zn.[29] Waste-derived mesoporous aluminosilicate (MAS) is environmentally friendly, has a high surface area and a narrow-distributed pore size, and a surface that can be easily tailored. All these features make it a suitable nanomaterial to serve as a COP-FBC carrier for the adsorption of Ba^{2+} as well as for the recovery of boron ion by crystallization of barium perborate, although MAS has never been used for this scope yet.

In this study, the mesoporous aluminosilicate (MAS) nanomaterial fabricated from the waste TFT-LCD panels serves as a carrier of COP-FBC to enhance the adsorption capacity of Ba^{2+} and the crystallization efficiency of boron. Moreover, the boron-containing precipitates are then calcined to form crystalline materials for the recovery of boron. As shown in Scheme 1, the waste TFT-LCD panel is melted at 1000 °C in the presence of Na_2CO_3 to produce hydroxyl-functionalized MAS, which can enhance the adsorption of Ba^{2+} by ion exchange. Ba-MAS is then used as a carrier in the COP-FBC reactor to provide the crystallization affinity toward boron recovery via the formation of barium peroxoborate ($BaB_2(OO)_2(OH_4)$) precipitates in the presence of H_2O_2. The identification of the crystallized phase change in the morphology of Ba-MAS before and after COP-FBC indicates that boron can be recovered as a high purity of BaB_2O_4. Results of this study clearly demonstrate the feasibility of using novel MAS from the waste TFT-LCD panel for the enhanced recovery of boron elements in wastewater, which can open a gateway to design an environmentally friendly treatment technology from the industrial wastes to simultaneously recover metal ions and inorganics.

■ RESULTS AND DISCUSSION

Surface Characterization of Silica Sand and MAS. The surface morphologies of commercial silica sand and the as-prepared MAS were first characterized and compared by electronic microscopic images. As illustrated in Figure 1a, the scanning electron microscopy (SEM) image of silica sand shows a well-rounded pattern with a smooth, fractured, irregularly cratered, and nonporous surface. The original waste TFT-LCD material shows large fragments with an unmelted and nonporous surface (Figure S1, Supporting Information). This large fragment is mainly from the angular flaky particles within a broad range of particle size after ball milling.[30] The SEM image of MAS after alkali treatment with Na_2CO_3 at 1000 °C is given in Figure 1b, which shows many roughly small particles with a multilayered assembly. The particle size of MAS, produced after the alkali and heat treatment, is in the range of 0.2−9.0 μm. Moreover, the cross-sectional field emission transmission electron microscopy (FE-TEM) images of MAS was further studied from the red box of Figure 1b to elucidate the change in surface morphology, and the result is shown in Figure 1c. It is clear that a wide range of nanostructured particles appear on the surface of MAS. In addition, the MAS shows a homogeneous distribution of nanoparticles on the surface, which form a hierarchical structure of aluminosilicate after Na_2CO_3 treatment and calcination at 600 °C for 6 h. As shown in Figure 1d, the distribution of MAS particles exhibits a narrow particle size range of 4−22 nm with an average lateral size of 12.8 ± 3.6 nm (n = 105), which indicates that MAS can provide a large specific surface area and pore channel to serve as a superior carrier for the recovery of boron species. It is noted that our previous study also used TFT-LCD to prepare the mesoporous aluminosilicate using the thermoalkaline reaction. The mean

DOI: 10.1021/acsomega.9b01900
ACS Omega 2019, 4, 14057−14066

particle size is 12.1 ± 3.9 nm after calcination at 110 °C for 12 h,[29] which is similar to the results obtained in this study.

Figure 2a shows Fourier transformation infrared (FTIR) spectra of silica and MAS after the alkali treatment at 1000 °C. The FTIR spectra of silica sand show a broad peak at 3502 cm^{-1}, which is the stretching vibration of the −OH bond and/or bending vibration of the adsorbed H−O−H bond from water molecules.[31] The peak at 1090 cm^{-1} belongs to Si−O−Si stretching, while that at 800 cm^{-1} in the silica sand spectra belongs to Si−O bending. After activation with Na_2CO_3, the MAS spectrum also exhibits a strong peak of hydroxyl functional group (−OH) at 3490 cm^{-1} and that of carbonyl group (C═O) at 1635 cm^{-1} in comparison with the silica sand. Another distinct peak located at 1007 cm^{-1}, which belongs to the $T-O^{-}\cdots Na^{+}$ bond, is originally derived from the cleavage of T−O−T′ linkages (where T and T′ is Si or Al)[32] at 1095 cm^{-1} (Figure S2, Supporting Information) after Na_2CO_3 activation.[33] Moreover, the X-ray diffractometer (XRD) patterns of MAS after activation treatment in the presence of Na_2CO_3 show several peaks at 13.9, 24.3, 30.1, 34.5, 38.1, 41.5, and 42.6°, which can be assigned to the (110), (211), (310), (222), (321), (400), and (411) planes of amorphous sodium aluminum carbonate silicate (ICDD-PDF-00-015-0469) (Figure S3, Supporting Information). The formation of amorphous silicate is mainly attributed to the fact that the aluminoborosilicate of TFT-LCD panel was blended with excess Na_2CO_3 during the melting process at a high temperature of 1000 °C.

The surface chemistry of silica sand and the as-prepared MAS was further studied to characterize the change in elemental species. Figure 2b shows the scan survey spectra of silica sand and acid-treated TFT-LCD panels of MAS nanomaterials. Several XPS peaks at 102, 153, 284, and 532 eV appear in the commercial silica sand spectra, which can be assigned to Si 2p, Si 2s, C 1s, and O 1s, respectively. This result clearly indicates that the silica sand only contains SiO_2. The small peak of C 1s at 284 eV is mainly attributed to trace organic carbons from the atmosphere. Moreover, several additional peaks centered at 74, 347, 1073, and 1304 eV are clearly observed in the MAS spectrum, which are mainly contributed from Al 2p, Ca 2p, Na 1s, and Mg 1s, respectively. The distinct peak of sodium atoms at 1073 eV can be assigned to the $Si-O-Na^{+}$ bond.[34] Our previous study has reported that the $Na_2O-B_2O_3$ phase can be removed during the activation process, and then the exposure of oxygen atoms would produce Si−OH or $Si-O\cdots Na^{+}$ functional group after acid washing.[29] Therefore, the borosilicate TFT-LCD waste can be completely tailored as the sodium aluminosilicate framework of MAS after the activation.

Pore Texture of Aluminosilicate Materials. The pore texture including specific surface areas and pore size distribution of silica sand and MAS was further examined. As illustrated in Figure 2c, the N_2 adsorption−desorption isotherm of the silica sand material can be classified as a type III isotherm with a slight hysteresis loop at a relative pressure range (P/P_0) of 0.9−0.95.[35] In addition, no obvious pore size distribution pattern is observed (Figure 2d). This result clearly indicates the nonporous nature of silica sand, and the hysteresis loop at a high P/P_0 range is mainly attributed to the interparticle voids of silica sand. In contrast to silica sand materials, the adsorption−desorption isotherm of MAS material follows a type IV physisorption isotherm with an H3 hysteresis loop in the P/P_0 range of 0.4−0.98, which is mainly attributed to the capillary condensation in mesoporous structures.[36] Moreover, the pore size distribution of MAS exhibits a sharp peak at 3.9 nm and then follows a broad pore size distribution in the mesoporous region (2−50 nm). The peak of 3.9 m is mainly attributed to the hierarchically pore structure of nanoparticles, while the broad distribution is from the voids of the interparticles of MAS. Moreover, the specific surface area is 0.6 m^2/g for the commercial silica sand and 226 m^2/g for MAS after the activation from waste TFT-LCD (Table S1, Supporting Information), which indicates that the activated MAS can serve as a potential carrier for COP-FBC treatment.

Adsorption of Ba^{2+} by MAS. The adsorption efficiency of barium ions by the treated TFT-LCD panel-based material (MAS) was investigated at pH 5. The selection of a weakly acidic condition is to avoid the precipitation of Ba^{2+} in solution. Figure 3 shows the adsorption isotherm of Ba^{2+} by silica sand and mesoporous MAS materials at 25 °C. The silica sand material exhibits little capacity for Ba^{2+} adsorption, probably attributed to the low specific surface area and the lack of functional groups. On the contrary, the mesoporous MAS material is an excellent adsorbent of Ba^{2+} in comparison with silica sand. The adsorption of Ba^{2+} ion by MAS increases dramatically at a low equilibrium concentration of <50 mg/L and then levels off to a plateau in a high equilibrium concentration range of 75−250 mg/L.

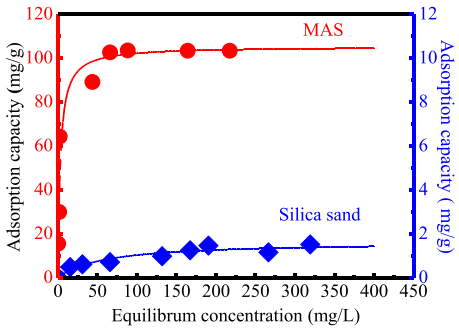

Figure 3. Adsorption isotherms and the fitted Langmuir model of silica sand and MAS for Ba^{2+} adsorption.

The adsorption behavior of divalent metal ions onto mesoporous material can be described by Langmuir and Freundlich isotherm models.[37] Table 1 shows the fitted parameters of Langmuir and Freundlich models. The Langmuir isotherm model can accurately describe the adsorption of Ba^{2+} by MAS mesoporous material, and the correlation coefficient (R^2) is >0.995. Moreover, the maximum adsorption capacity of Ba^{2+} is 105 mg/g. A previous study has used the surface-modified 2D titanium carbide to enhance the adsorption of barium ions, and the adsorption capacity of Ba^{2+} was 46.5 mg/g,[38] clearly indicating the superior ability of the developed MAS nanomaterials toward metal ion adsorption.

Table 1. Isothermal Parameters of Ba^{2+} Adsorption onto the Silica Sand and MAS Materials

	Langmuir model			Freundlich model		
material	q_{max} (mg/g)	K_d (L/mg)	R^2	K_f	n	R^2
silica sand	1.83	0.333	0.919	3.37	161	0.864
MAS	105	0.014	0.999	4.36	3.71	0.863

DOI: 10.1021/acsomega.9b01900
ACS Omega 2019, 4, 14057−14066

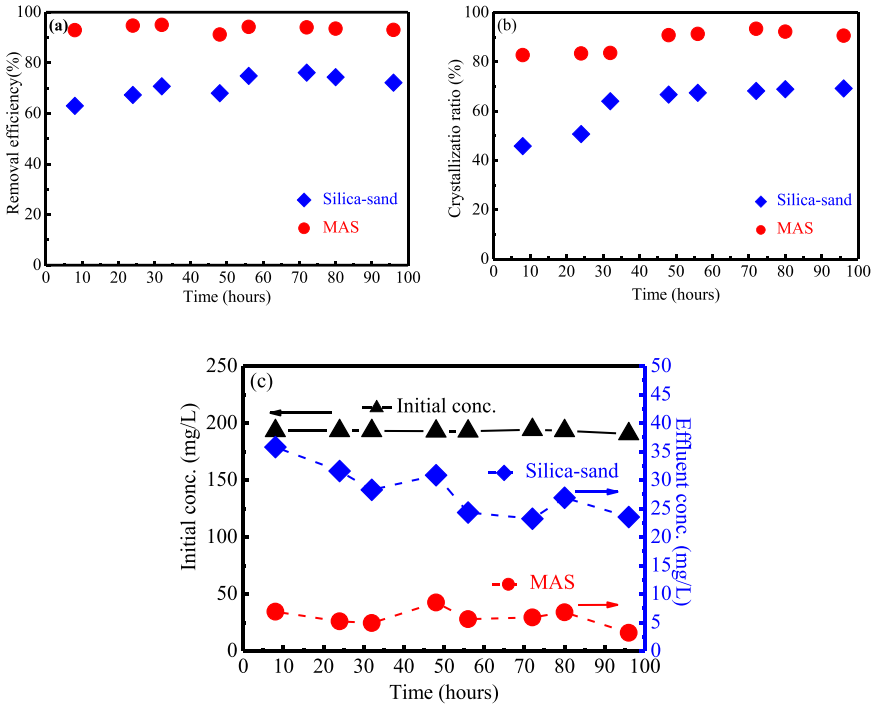

Figure 4. Comparison of the boron recovery performance of silica sand and MAS in terms of (a) removal efficiency, (b) crystallization ratio, and (c) effluent concentration as the function of reaction time in the COP-FBC process at pH 10.5.

Table 2. Comparison of the Recovery Efficiency and Crystallization Ratio of Boron Using COP-Based Treatment Processes

methods	$[B]_{in}$ (mg/L)	removal efficiency (%)	crystallization ratio (%)	pH	references
COP	1000	98.5	[a]	10 (batch)	17
COP	1000	99.7		10.5 (batch)	14
COP	1000	87		11 (batch)	15
FBHC	1000	96.6	60	11 (column)	15
FBC-silica sand	200	76.5	63	10.5 (column)	this study
FBC-MAS	200	94.8[b]	93.4		
	200	84.5[c]	93.4		

[a]No crystallization occurred. [b]Recovery that does not take into account the boron produced from the activation of TFT-LCD. [c]Recovery that takes into account the boron produced from the activation of TFT-LCD.

The high adsorption efficiency of Ba^{2+} by MAS can be attributed to the high mesoporosity and the functionalization of MAS during the activation process, which can not only produce a mesoporous structure for the removal of $Na_2O-B_2O_3$ phase structure but also increase the functional groups and electrostatic sites for Ba^{2+} adsorption. The negatively charged functional groups on the surface of aluminosilicate ($T-O^-$) can be counter-balanced by the addition of Na^+ cations from the activation agent of Na_2CO_3 to form $T-O^-\cdots Na^+$ clusters.[29] Besides, Ca^{2+} and Mg^{2+}, serving as charge compensators of AlO_4^- clusters, would migrate into the aluminosilicate surface when the Al-containing tetrahedral network is ruptured.[32] Therefore, the negatively charged surface and mesoporous structure of MAS enhance the adsorption of Ba^{2+} onto MAS, which may provide high affinity toward the nucleation of barium peroxoborate precipitate during the boron recovery in the COP-FBC process.

Boron Recovery by COP-FBC. Since the adsorbed Ba^{2+} onto the MAS may increase the crystallization of borate precipitates, the recovery efficiency as well as the crystallization ratio of boron by silica sand and MAS was used to evaluate the performance of COP-FBC process on boron recovery at the $[H_2O_2]/[B]$ and $[Ba]/[B]$ ratios of 2 and 1, respectively, at pH 10.5. Figure 4a shows the recovery efficiency of boron by silica sand and MAS as a function of reaction time in the COP-FBC process. It is clear that the recovery efficiency of boron by the commercial silica sand increases slightly from 62.9% at 10 h of incubation to 76.1% at 100 h. The MAS exhibits a better and stable recovery efficiency of boron, and the efficiency of 91.2−94.8% is observed after 100 h of incubation.

The crystallization ratio also shows a similar trend. As illustrated in Figure 4b, the crystallization ratio of boron increases from 45.8% at 10 h to 69.2% at 100 h by silica sand, while the crystallization ratio of 82.7−93.4% is observed when MAS was used as the carrier. A previous study has used the COP-FBC process to recover boron in the absence of a carrier and obtained a crystallization recovery of around 60%.[15] In this study, the high crystallization ratio of boron ions is mainly attributed to the high surface area of MAS and the high adsorbed amount of Ba^{2+} onto the surface, which can easily facilitate the nucleation and subsequently results in fast crystallization within 10 h. Therefore, the high crystallization property of MAS adsorbents produces less sludge in comparison with the commercial silica sand. In addition, the

DOI: 10.1021/acsomega.9b01900
ACS Omega 2019, 4, 14057−14066

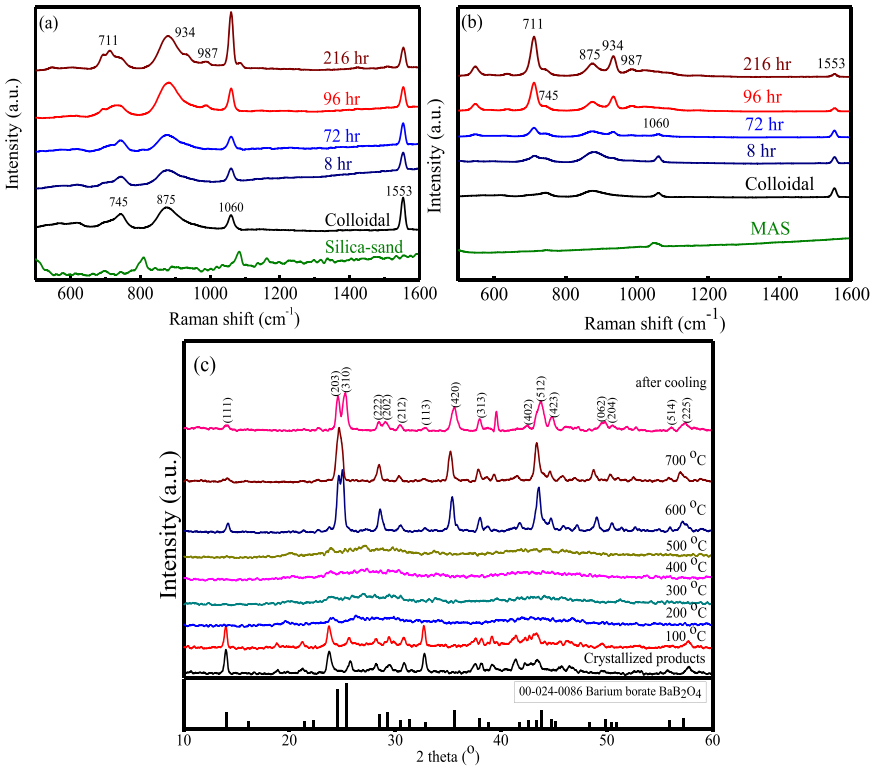

Figure 5. Raman spectra of the precipitates produced from the recovery of boron in the presence of (a) silica sand and (b) MAS as a function of reaction time. (c) HT-XRD patterns for crystallized products by MAS carrier in COP-FBC after 216 h of incubation.

boron concentration in the effluent can be maintained at a relatively low level in the presence of MAS. As shown in Figure 4c, the boron concentration in the effluent of the COP-FBC process decreases from 35.8 mg/L at 10 h to 23.5 mg/L at 100 h. In contrast, the boron concentration in the effluent decreases rapidly to 6.5 mg/L in the first 10 h and then maintains at the similar concentration after 100 h of incubation, clearly demonstrating the superiority of MAS for boron recovery and crystallization.

A wide variety of COP processes including pure COP and COP-FBHC in the absence of a carrier have been used to remove/recover boron in aqueous solutions.[14,15,17] Table 2 compares the recovery efficiency and crystallization ratio of boron with the reported results. Lin et al. investigated the effectiveness of boron recovery by COP using H_2O_2 and barium ions as promoters[14] and found that peroxoborate precipitates were transformed from the amorphous $BaB(OH)_3OOB(OH)_3$ and $Ba(B(OH)_3OOH)_2$ to the crystalline $BaB(OH)_2(OO)_2B(OH)_2$. Vu et al. used COP-FBHC to reclaim boron as the calcium perborate pellets to minimize the production of sludge and calculated the crystallization ratio to be around 60%.[15] Moreover, Shih et al. added H_2O_2 into the COP system to promote the treatment efficiency of boric acid in the presence of barium ions and obtained an enhanced boron removal efficiency of 98.5%.[17] Although good recovery efficiency of boron by COP-FBHC is observed, the crystallization ratio is not high and a large amount of sludge is produced, which needs further treatment and recycling.

In this study, the addition of MAS into the COP-FBC reactor shows a similar recovery efficiency of boron but a high crystallization ratio in comparison with those reported for COP and COP-FBHC processes,[14,15] clearly indicating that MAS is an excellent carrier to promote the precipitation of borate species as well as to enhance the crystallization ratio. The high crystallization ratio can be attributed to the high porosity and functionalization of MAS materials during the activation process, which enhance the ion exchange and electrostatic attraction sites to facilitate a strong interaction between barium ions and diperoxodiborate dianion ($B_2(OO)_2(OH)_4^{2-}$). Therefore, boron species can be recovered through the formation of barium peroxoborate. It should be noted that the original TFT-LCD glass contains boron as $N_2O-B_2O_3$, which is washed away during the activation process. Therefore, MAS itself would produce certain amount of boron that is supposed to be recovered by COP-FBC. This decreases the recovery of boron by COP-FBC from 94.8% originally to 84.5% when taking into account the total washed amount of boron from TFT-LCD. Since the boron species in COP-FBC will be recovered and crystallized, the MAS can, therefore, be recycled and reused for the sustainable removal of boron from wastewater.

Identification of Peroxoborate Precipitates. Since boron in solution can be reacted with barium ions to form peroxoborate precipitates in the presence of H_2O_2, the change in the chemical structure as well as the crystallinity of precipitates at various reaction times was further identified using Raman spectroscopy and high-temperature XRD. Figure 5a,b shows Raman spectra of the precipitates produced from reactions based on silica sand and MAS, respectively, at various reaction times. The Raman spectra of the precipitates from the silica sand shows four distinct peaks at 745, 875, 1060, and 1553 cm^{-1}. The peak at 875 cm^{-1} is the contribution of the symmetric BO_3 stretching of $B(OH)_3$ and O−O stretching of H_2O_2[13,39] and the band at 1553 cm^{-1} is attributed to the O−O stretching of oxygen.[14,15] Bands at 745 and 1060 cm^{-1} likely arise from the asymmetric $[B(OH)_4]^-$ stretching of

DOI: 10.1021/acsomega.9b01900
ACS Omega 2019, 4, 14057−14066

metaborate due to the υ_1 symmetric (B−O(OH)) of metaborate[14] and symmetric (B−OH) stretching of H_3BO_3,[40] respectively. This means that the precipitate from silica sand is an amorphous perborate and the chemical structure is $B(OH)_3(OOH)^-$.[14] It is clear that the peak intensities at 875 and 1060 cm^{-1} increase upon increase in the reaction time, which means an increase in the crystallization of the precipitates with time.

The Raman spectra of the precipitates produced from the MAS system are different from those from silica sand. Although the bands in the Raman spectra of the precipitates produced by MAS are similar to those by silica sand, the crystallization of MAS-based precipitates is more rapid and several sharp peaks at 711, 934, and 987 cm^{-1} associated with υ_{asym} ($B_2(OO)_2$), υ_{sym} (O−O), and υ_{sym} (B−O) are observed, respectively.[14,39] In addition, the peak intensity increases with increase in the reaction time from 8 to 216 h, which indicates that the reaction of perborate with peroxo groups produces cyclic dimeric peroxoborate $(B_2(OO)_2(OH)_4)^{2-}$ by linking two peroxo bridges with two four-coordinated boron atoms.[14,39] It is noteworthy that the crystalline structure of barium peroxoborate ($BaB_2(OO)_2(OH)_4$) is rapidly formed in the presence of MAS carrier because of considerable absorbed amounts of barium onto the MAS surface. These results clearly demonstrate the superiority of MAS to rapidly produce crystallized precipitates within 8 h in comparison with silica sand, which needs 216 h for crystallization.

To further understand the possible structure of the recovered precipitates, high-temperature XRD (HT-XRD) was further used to in situ identify the change in the crystallization of MAS-based products at various temperatures. As illustrated in Figure 5c, HT-XRD patterns show that the structure of peroxoborate ($BaB_2(OO)_2(OH)_4$) changes from a well-crystallized phase originally to an amorphous phase at 200−500 °C. However, the crystallinity of BaB_2O_4 changes again when the samples are sintered to 600 °C. The lattice constants of a = 11.13 Å, b = 12.67 Å, and c = 8.38 Å are obtained, which is the $C2/c$ space group of BaB_2O_4 (ICDD-PDF-00-024-0086). In this study, the boron-based precipitate is calcined at 1050 °C and a glasslike material is obtained, which indicates the formation of α-BaB_2O_4 structure.

Crystallization Mechanism. To further elucidate the mechanism of crystallization, the change in the morphology of boron-containing precipitates by silica sand and MAS materials was further examined by cross-sectional SEM. As illustrated in Figure 6, the needle-shaped precipitates of perborate start to accumulate onto the active sites of the MAS surface at 8 h (Figure 6a) and then almost cover the surface of MAS at 72 h (Figure 6b). Once the formation of perborate precipitates reaches the saturation of active sites onto the MAS surface, the crystals start to build up the peroxo-bridge and continue to grow to generate a multilayered structure at 96 h (Figure 6c). Finally, the MAS surface exhibits a layer-by-layer assembly to form a core−shell structure at 216 h (Figure 6d). Moreover, the monoclinic crystal length of barium peroxoborate is in the range of 10−20 μm (inset of Figure 6d). It is also noted that the SEM−EDS spectrum only shows peaks of Ba, B, and O elements onto MAS after 216 h (Figure S4, Supporting Information), which depicts the formation of α-BaB_2O_4 onto the MAS surface.

Figure 6e−h shows the evolution of crystallization of the silica sand at various reaction times. Different from the MAS system, small amount of precipitate is produced onto the silica sand surface up to 72 h. The precipitation of spherically colloidal particles onto the silica sand surface is observed at 96 h and then accumulates on the surface after 216 h of reaction. The difference in the formation mechanisms of boron precipitates between silica sand and MAS is mainly attributed to the surface functionality and specific surface area. MAS contains functional groups including Si−OH^- active sites and negatively charged ions of T−O^-···Na^+ on the surface.[29,34] The large surface area of MAS can thus provide abundant ion exchange sites and negative charges to capture Ba^{2+} from the aqueous solution, which can, in turn, produce a highly crystalline barium peroxoborate ($BaB_2(OO)_2(OH)_4$) through a dimeric peroxoborate anion $(B_2(OO)_2(OH)_4)^{2-}$.

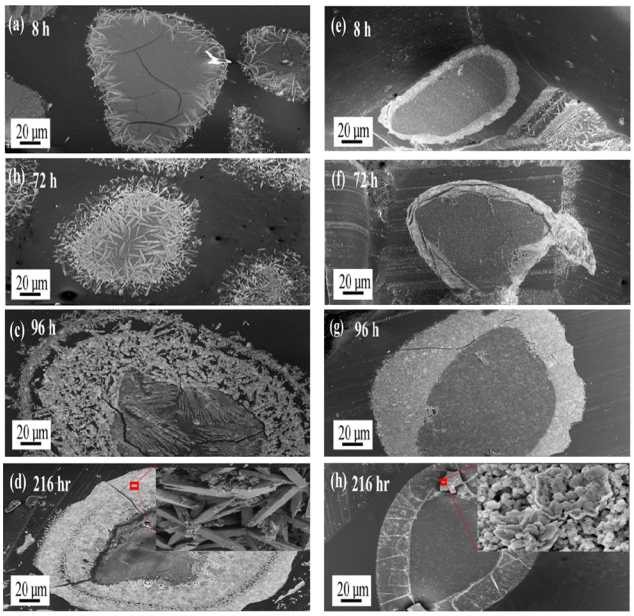

Figure 6. Cross-sectional SEM images of (a−d) MAS and (e−h) silica sand during boron recovery at various reaction times.

According to these results, the possible mechanism of the crystallization and recovery of boron in the presence of silica sand and MAS materials is proposed. As illustrated in Scheme 2, the crystallization of peroxoborate species in the presence of silica sand occurs from the homogeneous nucleation to produce flowerlike spherical crystals with a diameter of around 2 μm. The attachment of colloidal particles onto silica sand would then result in collision between nuclei and silica sands, resulting in heterogeneous nucleation and granulation. A wide variety of FBC reactions using silica sand as carriers for the removal of metal and nonmetal ions in aqueous solution also show similar reaction mechanism.[41] Since silica sand lacks high surface area to enhance nucleation, long crystallization time is needed and a large amount of sludge would be produced during coagulation/flocculation processes. In contrast, the Ba^{2+}-adsorbed MAS triggers the formation of barium peroxoborate more readily, followed by the nucleation and crystallization to produce a needle-like crystalloid. The needle-like crystalloid grows directly on the rough surface along with open pores of MAS. Once the active sites reach saturation, the crystalline precipitates start to grow layer-by-layer by the formation of oxo-bridge and subsequently result in the formation of a core−shell structure.

DOI: 10.1021/acsomega.9b01900
ACS Omega 2019, 4, 14057−14066

Scheme 2. Conceptual Model of the Crystallization of Barium Peroxoborate in the COP-FBC Reactor Using Silica Sand and Mesoporous MAS Nanomaterials as Carriers

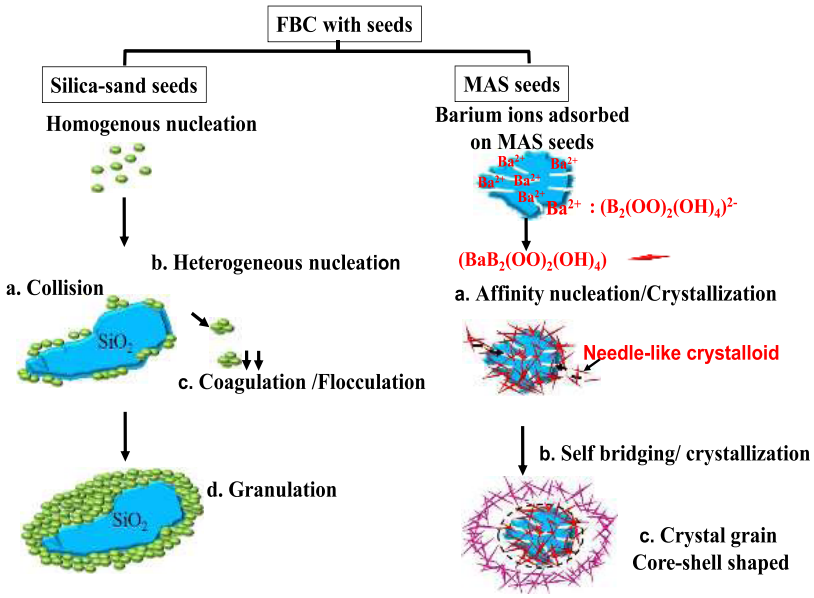

CONCLUSIONS

In this study, a functionalized mesoporous MAS nanomaterial previously developed from the TFT-LCD panel waste glass serves as a sustainable carrier for the adsorption of barium ions as well as the recovery of boron. The nonporous waste glass is transformed into mesoporous aluminosilicate nanomaterials via the cleavage of passive Si−O−BO bonds into the reactive Si−O linkages and negatively charged ions of $T-O^{-}\cdots Na^{+}$ on the surface. A high surface area of 226 m^2/g is also obtained for MAS after activation. MAS exhibits an excellent capacity for barium adsorption, and the maximum adsorption of 105 mg/g is observed, which enhances the recovery efficiency and crystallization ratio of boron by 95 and 93.4%, respectively. Moreover, the possible mechanisms for the crystallization of boron-containing precipitates are elucidated. The surface functionality and large surface area of MAS trigger the crystallization of precipitates more readily and produce a layer-by-layer core−shell-type crystals rapidly. HT-XRD confirms that the crystallinity of the end-product of MAS crystallization is a hexagonal-phase BaB_2O_4, which is then converted to α-BaB_2O_4 at 1050 °C. Results obtained in this study clearly demonstrate a novel environmentally benign strategy for the fabrication of functionalized mesoporous aluminosilicate as the COP-FBC carrier, which can open a gateway to recover boron species from water and wastewater after the calcination of boron-containing precipitates.

EXPERIMENTAL SECTION

Chemicals. Sodium carbonate (Na_2CO_3, >99.5%), NaOH, $BaCl_2$, HBO_3, and H_2O_2 were purchased from Merck Co. Hydrochloric acid (HCl, EL grade) and nitric acid (HNO_3, EL grade) were obtained from BASF Co. All the other chemicals used in this study were of analytical grade and used as received without further purification. The waste TFT-LCD panel, an aluminoborosilicate glass,[42] was from a local TFT-LCD company (Hsinchu, Taiwan). All solutions were prepared using distilled deionized water (18.2 MΩ cm) unless otherwise mentioned.

Preparation of MAS. The MAS adsorbent was prepared from the waste TFT-LCD panel according to our previous study with minor modification.[29] Briefly, TFT-LCD was ball-milled for 1 h and then blended with Na_2CO_3 for 10 min at a ratio of 1:3 to fabricate the functionalized mesoporous materials. It is noteworthy that the melting point of aluminoborosilicate is up to 1500 °C, which can be reduced to 1000 °C with the addition of Na_2CO_3. Therefore, the resultant mixture was melted at 1000 °C for 10 min in a furnace. After cooling to room temperature, the resultant material was acid-washed with 1.0 N HCl repeatedly until the solution pH was around 7. Finally, the obtained mesoporous aluminosilicate nanomaterial, denoted as MAS, was calcined in the furnace at 600 °C for 6 h and then stored in a desiccator for further use.

Characterization of Silica Sand and MAS. The pore texture and surface area of silica sand, the commercial carrier commonly used in the COP-FBC process, and MAS were characterized by N_2 adsorption−desorption isotherm using a micromeritics system model ASAP 2420 surface area analyzer over a relative pressure (P/P_0) range of 0.01−0.99 at 77 K. The material was degassed at 150 °C for 6 h in a vacuum to remove moisture prior to analysis. The specific surface area (S_{BET}) was determined over the P/P_0 range of 0.05−0.2 using the Brunauer−Emmett−Teller (BET) equation. The total pore volume (V_t) was calculated at a relative pressure of 0.989. Moreover, the pore size distribution was analyzed by the Barrett−Joyner−Halenda model.

The surface morphology as well as the cross-sectional image of aluminosilicate materials was examined by field-emission scanning electron microscopy (Zeiss LEO 1530 FE-SEM) coupled with energy-dispersive X-ray spectroscopy (EDS) (Bruker, XFlash Dector 5010) at 20 kV and field emission transmission electron microscopy (FE-TEM, JEOL JEM-2100F/OXFORD X-Max 80T) at 200 kV. The cross section of aluminosilicate materials was prepared using a rotary microtome (Leica Ultracut, Germany). Moreover, the histogram of MAS was determined by counting the particle size from the FE-TEM image. The crystallinity was identified by

DOI: 10.1021/acsomega.9b01900
ACS Omega 2019, 4, 14057−14066

using a Bruker D8 advanced X-ray diffractometer (XRD) with a Cu Kα radiation (λ = 1.5405 Å) at the voltage and current density of 40 kV and 40 mA, respectively. The change in chemical species of element in MAS nanomaterials was analyzed by a ESCA PHI 1600 X-ray photoelectron spectrometer (XPS, Physical Electronics, Eden Prairie, MN) using an Al Kα X-ray source at 1486.6 eV. The crystalline structure of boron-containing precipitate was determined by high-temperature X-ray diffraction (HT-XRD) (Multiflex, Rigaku, Tokyo, Japan) with a Cu Kγ radiation at 40 kV and 40 mA. The XRD patterns of the precipitate were recoded from 100 to 700 °C in air on a Pt stage. The Raman spectra of crystal functional were recorded by a Bruker Senterra micro-Raman spectrometer equipped with an Olympus BX 51 microscope and a DU420-OE CCD camera. The functional groups of aluminosilicate-based nanomaterials were determined with a Horiba FT720 Fourier transformation infrared (FTIR) spectrophotometer to confirm the functional groups of the as-prepared MAS nanomaterials.

Adsorption of Barium Ions by MAS. The adsorption of barium ions by the as-prepared MAS was performed in batch experiments. After the addition of 1 g/L the as-prepared MAS into 100 mL of solutions containing 10−300 mg/L barium ions at pH 5, the suspensions were incubated isothermally at 25 °C on a reciprocating thermostat water bath shaker at 150 rpm for 24 h in the dark. Appropriate amount (1 mL) of solution was sampled at the specific intervals and the solution was filtrated by 0.45 μm filters to separate liquids and solids. The initial and final concentrations of barium ions in solutions were measured by an inductively coupled plasma-optical emission spectrophotometer (ICP-OES, iCAP-7400, Thermo Fisher).

COP-FBC Experiments. The recovery of boron by the as-synthesized MAS and the commercial silica sand were studied in COP-FBC experiments. As shown in Figure S5 (Supporting Information), 50 g/L of the as-synthesized MAS and silica sand was added into each COP-FBC column. Three different synthetic solutions containing boron, barium, and H_2O_2 at flow rates of 15, 15, and 0.7 mL/min, respectively, were transferred into the mixture separately to yield the $[H_2O_2]/[B]$ and $[Ba]/[B]$ ratios of 2 and 1, respectively, at pH 10.5.[14] To monitor the change in boron concentration in the COP-FBC reactor, 100 mL of effluent was sampled at regular intervals and then filtrated by 0.45 μm filters to separate liquids and solids. The boron concentration in effluent solutions was determined by ICP-OES. In addition, the efficiency of COP-FBC was evaluated by recovery efficiency (RE, %) and crystallization ratio (CR, %) of boron using eqs 1 and 2.[15,43,44]

$$\mathrm{RE}\ (\%) = \left(1 - \frac{[B]_s \times Q_t}{C_{B0} \times Q_{B-AW_B}}\right) \quad (1)$$

$$\mathrm{CR}\ (\%) = \left(1 - \frac{[B]_t \times Q_t}{C_{B0} \times Q_B}\right) \quad (2)$$

where $[B]_s$ and $[B]_t$ are the boron concentrations in the effluent and carrier, respectively; Q_t and Q_B are the total flow rate and boron flow rate, respectively; C_{B0} is the initial boron concentration; and AW_B is the total amount of boron washed from TFT-LCD during activation process.

■ ASSOCIATED CONTENT

Supporting Information

The Supporting Information is available free of charge on the ACS Publications website at DOI: 10.1021/acsomega.9b01900.

Illustration of the experimental setup of COP-FBC; SEM images and FTIR spectrum of waste TFT-LCD material; XRD patterns of MAS; and EDS spectra of MAS (PDF)

■ AUTHOR INFORMATION

Corresponding Author

*E-mail: radoong@mx.nthu.edu.tw. Tel: +886-3-5726785. Fax: +886-3-5718649.

ORCID

Yoshikazu Suzuki: 0000-0002-4418-6893

Ruey-an Doong: 0000-0002-4913-0602

Author Contributions

The manuscript was written through contributions of all authors. All authors have given approval to the final version of the manuscript.

Notes

The authors declare no competing financial interest.

■ ACKNOWLEDGMENTS

The authors thank the Ministry of Science and Technology (MOST), Taiwan, for financial support under Grant Nos. MOST 107-2221-E-007-113-MY3 and 107-2911-I-007-302.

■ REFERENCES

(1) Bodzek, M. The Removal of Boron from the Aquatic Environment- State of the Art. *Desalin. Water Treat.* **2016**, *57*, 1107−1131.

(2) Wolska, J.; Bryjak, M. Method for Boron Removal from Aqueous Solution - A review. *Desalination* **2013**, *310*, 18−24.

(3) Fang, Y.; Wang, X. Metal-Free Boron-Containing Heterogeneous Catalysts. *Angew. Chem., Int. Ed.* **2017**, *56*, 15506−15518.

(4) Hu, J.; Pu, Y.; Ueda, M.; Zhnag, X.; Wang, L. Charge-Aggregate Induced (CAI) Reverse Osmosis Membrane for Seawater Desalination and Boron Removal. *J. Membr. Sci.* **2016**, *520*, 1−7.

(5) Guan, Z.; Lv, J.; Bai, P.; Guo, X. Boron removal from aqueous solution by dasorption −A review. *Desalination* **2016**, *383*, 29−37.

(6) Sari, M. A.; Shankararaman, C. Mechanism of Boron Removal from Hydraulic Fracturing Wastewater by Aluminum Electrocoagulation. *J. Colloid Interface Sci.* **2015**, *458*, 103−111.

(7) Irawan, C.; Kuo, Y. L.; Liu, J. C. Treatment of Boron-Containing Optoelectronic Wastewater by Precipitation Process. *Desalination* **2011**, *280*, 146−151.

(8) Kartikaningsih, D.; Huang, Y. H.; Shih, Y. J. Electro-Oxidation and Characterization of Nickel Foam Electrode for Removing Boron. *Chemosphere* **2017**, *166*, 184−191.

(9) Dolati, M.; Aghapour, A. A.; Khorsandi, H.; Karimzade, S. Boron Removal from Aqueous Solutions by Electrocoagulation at Low Concentrations. *J. Environ. Chem. Eng.* **2017**, *5*, 5150−5156.

(10) Arias, M. F. C.; i Bru, L. V.; Rico, D. P.; Galvan, P. V. Comparison of Ion Exchange Resin Used in Reduction of Boron in Desalinated Water for Human Consumption. *Desalination* **2011**, *278*, 244−253.

(11) Bilgin Simsek, E.; Beker, U.; Senkal, B. F. Predicting the Dynamics and Performance of Selective Polymeric Resins in A Fixed Bed System for Boron Removal. *Desalination* **2014**, *349*, 39−50.

(12) Kang, J.; Tang, Y.; Gao, S.; Liu, L. One-Dimensional Controllable Cross-linked Polymers Grafted with N-Methyl-D-

DOI: 10.1021/acsomega.9b01900
ACS Omega 2019, 4, 14057−14066

Glucamine for Effective Boron Adsorption. *New J. Chem.* **2018**, *42*, 11334−11340.
(13) Lin, J. Y.; Shin, Y. J.; Hsieh, T. Y.; Huang, Y. H. Role of Phase Transformation of Barium Perborates in the Effective Removal of Boron from Aqueous Solution via Chemical Oxo-Precipitation. *RSC Adv.* **2016**, *6*, 63206−63213.
(14) Lin, J. Y.; Shin, Y. J.; Chen, P. Y.; Huang, Y. H. Precipitation Recovery of Boron from Aqueous Solution by Chemical Oxo-Precipitation at Room Temperature. *Appl. Energy* **2016**, *164*, 1052−1058.
(15) Vu, X. T.; Lin, J. Y.; Shih, Y. J.; Huang, Y. H. Reclaiming Boron as Calcium Perborate Pellets from Synthetic Wastewater by Integrating Chemical Oxo-Precipitation within a Fluidized-Bed Crystallizer. *ACS Sustainable Chem. Eng.* **2018**, *6*, 4784−4792.
(16) Lin, J. Y.; Song, Y. J.; Shin, Y. J.; Huang, Y. H. Solubility Products of Sparingly Soluble Barium Perborates in Aqueous Solution that Contains $B(OH)_3$ and H_2O_2 at 25 °C. *J. Colloid Interface Sci.* **2017**, *505*, 703−710.
(17) Shih, Y. J.; Liu, C. H.; Lan, W. C.; Huang, Y. H. A Novel Chemical Oxo-Precipitation (COP) Process for Efficient Remediation of Boron Wastewater at Room Temperature. *Chemosphere* **2014**, *111*, 232−237.
(18) Shih, Y. J.; Abarca, R. R. M.; Luna, M. D. G.; Huang, Y. H.; Lu, M. C. Recovery of Phosphorus from Synthetic Wastewaters by Struvite Crystallization in a Fluidized-Bed Reactor: Effects of pH, Phosphate Concentration and Coexisting Ions. *Chemosphere* **2017**, *173*, 466−473.
(19) Jiang, K.; Zhou, K. G. Recovery and Removal of Fluoride from Fluorine Industrial Wastewater by Crystallization Process: A Pilot Study. *Clean Technol. Environ. Policy* **2017**, *19*, 2335−2340.
(20) Hernández-Morales, V.; Nava, R.; Acosta-Silva, Y. J.; Macias-Sanchez, S. A.; Perez-Bueno, J. J.; Pawelec, B. Adsorption of Lead (II) on SBA-15 Mesoporous Molecular Sieve Functionalized with−NH_2 Groups. *Microporous Mesoporous Mater.* **2012**, *160*, 133−142.
(21) Javadian, H.; Vahedian, P.; Toosi, M. Adsorption Characteristics of Ni (II) from Aqueous Solution and Industrial Wastewater onto Polyaniline/HMS Nanocomposite Powder. *Appl. Surf. Sci.* **2013**, *284*, 13−22.
(22) Doong, R. A.; Liao, C. Y. Enhanced Photocatalytic Activity of Cu-Deposited N-TiO_2/Titanate Nanotubes under UV and Visible Light Irradiations. *Sep. Purif. Technol.* **2017**, *179*, 403−411.
(23) Doong, R. A.; Liao, C. Y. Enhanced Visible-Light-Responsive Photodegradation of Bisphenol A by Cu, N-Codoped Titanate Nanotubes Prepared by Microwave-Assisted Hydrothermal Method. *J. Hazard. Mater.* **2017**, *322*, 254−262.
(24) Amato, A.; Rochetti, L.; Beolchini, F. Environmental impact assessment of different end-of-life LCD management strategies. *Waste Manag.* **2017**, *59*, 432−441.
(25) Amato, A.; Beolchini, F. End of life liquid crystal displays recycling: A patent review. *J. Environ. Manage.* **2018**, *225*, 1−9.
(26) Tsujiguchi, M.; Kobashi, T.; Utsumi, Y.; Kakimori, N.; Nakahira, A. Synthesis of Zeolite from Aluminoborosilicate Glass Used in Glass Substrates of Liquid Crystal Display Panels and Evaluation of its Cation Exchange Capacity. *J. Am. Ceram. Soc.* **2014**, *97*, 114−119.
(27) Kim, K.; Kim, K.; Hwang, J. Thin Film Transistor-Liquid Crystal Display Cullet: A Raw Material for Production of Commercial Soda Lime Silicate Glasses. *J. Cleaner Prod.* **2014**, *79*, 276−282.
(28) Li, X.; Gao, S.; Xing, P.; Dong, K.; Gao, B.; Feng, Z. Recovery and reutilization of high-quality boron carbide from sapphire wafer grinding-waste. *J. Environ. Manage.* **2018**, *224*, 106−112.
(29) Tsai, C. K.; Doong, R. A.; Hung, H. Y. Sustainable Valorization of Mesoporous Aluminosilicate Composite from Display Panel Glass Waste for Adsorption of Heavy Metal Ions. *Sci. Total Environ.* **2019**, *673*, 337−346.
(30) Jang, H.; Jeon, S.; So, H.; So, S. Properties of Different Particle Size of Recycled TFT-LCD Waste Glass Powder as A Cement Concrete Binder. *Int. J. Precis. Eng. Manuf.* **2015**, *16*, 2591−2597.
(31) Dutta Chowdhury, A.; Doong, R. A. Highly Selective and Selective Detection of Nanomolar Ferric Ions Using Dopamine Functionalized Graphene Quantum Dots. *ACS Appl. Mater. Interfaces* **2016**, *8*, 21002−21010.
(32) Ning, C.; Pejman, H.; Meng, X.; Lin, C. S.; McKay, K. G. Valorization of an Electronic Waste-Derived Aluminosilicate: Surface Functionalization and Porous Structure Tuning. *ACS Sustainable Chem. Eng.* **2016**, *4*, 2980−2989.
(33) Mikhailova, O.; del Campo, A.; Rovnanik, P.; Fernández, J. F.; Torres-Carrasco, M. In Situ Characterization of Main Reaction Products in Alkali-Activated Slag Material by Confocal Raman Microscopy. *Cem. Concr. Compos.* **2019**, *99*, 32−39.
(34) McGrail, B. P.; Icenhower, J. P.; Shuh, D. K.; Liu, P.; Darab, J. G.; Baer, D. R.; Thevuthasen, S.; Shutthanandan, V.; Engelhard, M. H.; Booth, C. H.; Nachimuthu, P. The Structure of Na_2O-Al_2O_3-SiO_2 Glass: Impact on Sodium Ion Exchange in H_2O and D_2O. *J. Non-Cryst. Solids* **2001**, *296*, 10−26.
(35) Hadi, P.; Barford, J.; Mckay, G. Toxic Heavy Metal Capture Using a Novel Electronic Waste-Based Material- Mechanism, Modeling and Comparison. *Environ. Sci. Technol.* **2013**, *47*, 8248−8255.
(36) Doong, R. A.; Tsai, C. W. Synergistic Effect of Cu Adsorption on the Enhanced Photocatalyst Degradation of Bisphenol a by TiO_2/Titanate Nanotubes Composite. *J. Taiwan Inst. Chem. Eng.* **2015**, *57*, 69−76.
(37) Jung, K. W.; Lee, S. Y.; Choi, J. W.; Lee, Y. J. A facile one-pot hydrothermal synthesis of hydroxyapatite/biochar nanocomposites: Adsorption behavior and mechanisms for the removal of copper (II) from aqueous media. *Chem. Eng. J.* **2019**, *369*, 529−541.
(38) Mu, W.; Du, S.; Yu, Q.; Li, X.; Wei, H.; Yang, Y. Improving Barium Ion Adsorption on Two Dimensional Titanium Carbide by Surface Modification. *Dalton Trans.* **2018**, *47*, 8375−8381.
(39) Lin, J. Y.; Shih, Y. J.; Chen, P. Y.; Huang, Y. H. Potential Oxo-Precipitation (COP) for Remediating Wastewater with a High Boron Concentration Using H_2O_2/$Ba(OH)_2$ at Room Temperature. *Energy Procedia* **2014**, *61*, 349−352.
(40) Walrafen, G. E.; Krishnan, P. N.; Hokmabadi, M. D.; Griscom, C.; Munro, R. G. Surface Raman Scattering from Effervescent Magnetic Peroxyborates. *J. Chem. Phys.* **1982**, *77*, 3840−3846.
(41) Chen, C. S.; Shih, Y. J.; Huang, Y. H. Remediation of Lead(Pb(II)) Wastewater Through Recovery of Lead Carbonate in as Fluidized-Bed Homogeneous Crystallization (FBHC) System. *Chem. Eng. J.* **2015**, *279*, 120−128.
(42) Tsujiguchi, M.; Kobashi, T.; Utsumi, Y.; Kakimori, N.; Nakahira, A. Synthesis of FAU Zeolite from Aluminoborosilicate Glass and Elution Behavior of Glass Components. *J. Ceram. Soc. Jpn.* **2014**, *122*, 104−109.
(43) Priambodo, R.; Shih, Y. J.; Huang, Y. H. Phosphorus Recovery as Ferrous Phosphate (Vivianite) From Wastewater Produced in Manufacture of Thin Film Transistor-Liquid Crystal Displays (TFT-LCD) by a fluidized bed crystallizer (FBC). *RSC Adv.* **2017**, *7*, 40819−40828.
(44) Villa-Gomez, D.; Ababneh, H.; Papirio, S.; Rousseau, D. P. L.; Lens, P. N. L. Effect of Sulfide Concentration on the Location of the Metal Precipitates in Inversed Fluidized Bed Reactors. *J. Hazard. Mater.* **2011**, *192*, 200−207.

DOI: 10.1021/acsomega.9b01900
ACS Omega 2019, 4, 14057−14066